MOLECULAR IMAGING AND BIOLOGY

Published Online: 28 July 2009

Mol Imaging Biol (2010) 12:145–154
DOI: 10.1007/s11307-009-0248-6

RESEARCH ARTICLE

Dynamic Contrast-Enhanced Folate-Receptor-Targeted MR Imaging Using a Gd-loaded PEG-Dendrimer–Folate Conjugate in a Mouse Xenograft Tumor Model

Wei-Tsung Chen,[1,2] Dhakshanamurthy Thirumalai,[3] Tiffany Ting-Fang Shih,[2,4] Ran-Chou Chen,[1,5] Shin-Yang Tu,[1] Chin-I Lin,[3] Pang-Chyr Yang[6,7]

[1]*Department of Radiology, Taipei City Hospital, Taipei, Taiwan*
[2]*Department of Radiology, School of Medicine, National Taiwan University, Taipei, Taiwan*
[3]*Union Chemical Laboratory, Industrial Technology Research Institute, Hsinchu, Taiwan*
[4]*Department of Medical Imaging, National Taiwan University Hospital, Taipei, Taiwan*
[5]*Department of Biomedical Imaging and Radiological Sciences, National Yang-Ming University, Taipei, Taiwan*
[6]*Department of Medicine, National Taiwan University Hospital, Taipei, Taiwan*
[7]*Department of Medicine, School of Medicine, National Taiwan University, Taipei, Taiwan*

Abstract

Purpose: The purpose of this study is to validate a folate-receptor (FR)-targeted dendrimer, PEG-G3-(Gd-DTPA)11-(folate)5, for its ability to detect FR-positive tumors, by using dynamic contrast-enhanced MRI.

Procedures: KB cells, FR siRNA knockdown KB cells, and FR negative HT-1080 cells, were incubated with fluorescein-labeled dendrimer and their cellular uptake was observed. Dynamic contrast-enhanced MRI was performed on mice-bearing KB and HT-1080 tumors and the enhancement patterns and parameters were analyzed.

Results: Green fluorescence was found in the KB cells in the cellular uptake experiment, but was not seen in other settings. In the dynamic contrast-enhanced MRI, the 30-min washout percentage was −4±18% in the KB tumors and 39±23% in the HT-1080 tumors. A 17% cut-off point gave a sensitivity of 94.4% and a specificity of 93.8%.

Conclusions: We have demonstrated the targeting ability of PEG-G3-(Gd-DTPA)11-(folate)5 *in vitro* and *in vivo*. A 17% cut-off point for a 30-min washout percentage can be a useful parameter for the diagnosis of FR-positive tumors.

Key words: Molecular imaging, Dendrimer, Folate receptor, MRI

Introduction

The folate receptor (FR) is overexpressed in several human tumors, including cancers of the ovary, uterus, colon, lung, and kidney [1–5]. Conjugates of folic acid linked via its gamma-carboxyl have the ability to enter receptor-expressing cancer cells via folate-receptor-mediated endocytosis [6, 7]. Because the affinity between folate and FR is high [8, 9] (the dissociation constant is approximately 10^{-10}M), folic acid conjugates allow the selective delivery of diagnostic or therapeutic agents to FR-expressing cancer cells in the presence of normal cells [8, 10, 11].

Molecular imaging is a new discipline that unites molecular biology and *in vivo* imaging. In previous receptor-targeted magnetic resonance (MR) imaging studies, authors usually

Electronic supplementary material The online version of this article (doi:10.1007/s11307-009-0248-6) contains supplementary material, which is available to authorized users.

Correspondence to: Tiffany Ting-Fang Shih; *e-mail:* ttfshih@ntu.edu.tw

compared the contrast enhancement ratio between the receptor-positive and the -negative tumors at various time points after contrast injection, and showed that the receptor-positive tumors had higher enhancement ratios and longer enhancement durations [12–18]. However, it is sometimes hard to scan exactly the same cross-sectional area before, and at different time points after contrast injection; thus, it is hard to get unbiased hemodynamic information from a certain portion of the tumor. Dynamic contrast-enhanced (DCE) MR has been used in clinical situation for years and it has the advantage of observing a part of tumor for certain time periods at different time points without moving the subject. This reveals the hemodynamic characteristics of the tumor. The enhancement pattern obtained from DCE is valuable for differential diagnosis of malignant and benign tumors [19, 20]. In this study, we tried to apply DCE in receptor-targeted MR imaging, and tried to analyze the enhancement pattern between receptor-expressing and receptor-negative tumors.

We recently synthesized a dendrimer with polyethylene glycol (PEG) core, which acts as a carrier bearing 16 functional hydroxyl groups for conjugating molecular probes and gadolinium chelates as a MR T1 contrast agent. Next, we conjugated folate and gadolinium-DTPA with the dendrimer as a FR receptor-targeting beacon. The purpose of this study was to use the FR receptor-targeting MR contrast agent to detect folate-receptor-positive cells *in vitro* and in a mouse xenograft tumor model. This was in order to determine if tumors of interest have such a specific target by analyzing the enhancement parameters obtained from dynamic contrast-enhanced MR imaging.

Materials and Methods

Contrast Medium

Hydroxy-terminated polyester dendrons were synthesized from the chain-ends of linear PEG and 2,2-bis(hydroxymethyl) propionic acid ranging from generations one to three according to a divergent approach [21]. A sequence of reactions, which included the anhydride-coupling step and subsequent deprotection by hydrogenolysis, was repeated until the G3 generation dendrimer with 16 hydroxyl functional groups was obtained. Then, the functional groups present at the surface of the dendrimers were utilized for the conjugation of folate moieties (average number = 5) as well as diethylenetriaminepentaacetate (DTPA; average number = 11). Later, the DTPA terminals were complexed with gadolinium ions (Fig. 1).

Preparation of Benzylidene-protected G_1 Generation of the PEG-dendrimer [PEG-bis[G-1]-(O_2Bn)] PEG diol (MW 4,000 Da, 9.2 g, 2.3 mmol, 1 eq) and 4-dimethylaminopyridine (DMAP; 0.1670 g, 0.39 mmol) were placed in a R.B. flask under nitrogen atmosphere and was added 25 mL of dichloromethane to dissolve the mixture. Benzylidene-2, 2-bis (oxymethyl) propionic (BOP) anhydride (4.27 g, 10 mmol) dissolved in dichloromethane (25 mL) was added drop wise to the above solution. The reaction mixture was then stirred

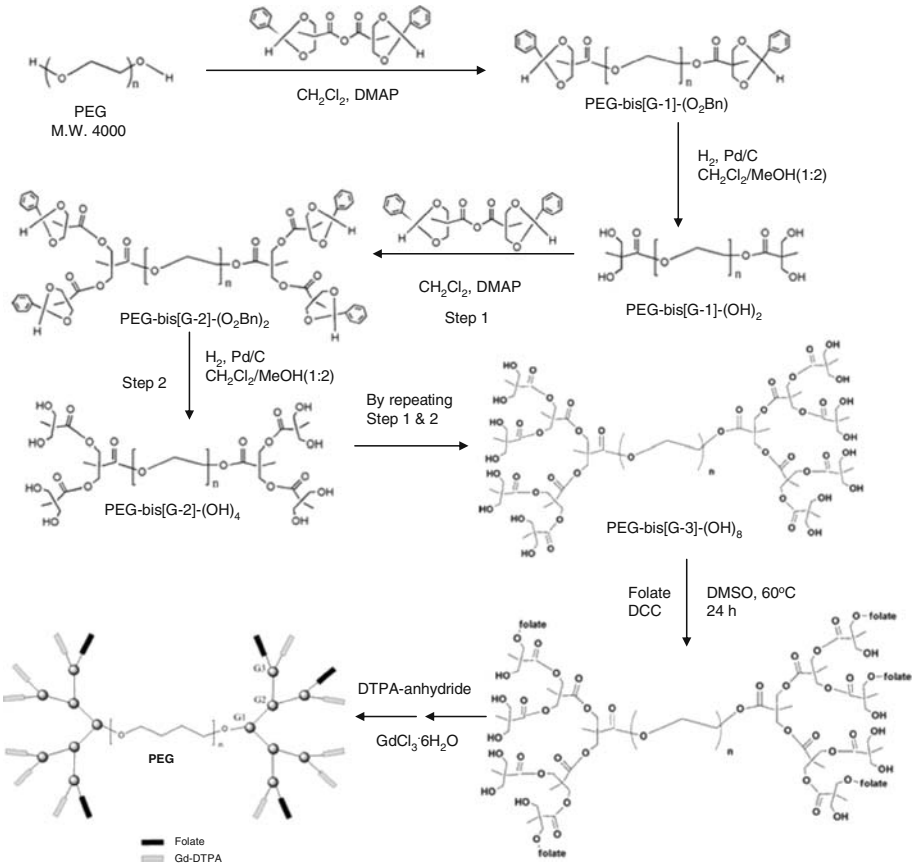

Fig. 1. The synthesis scheme of the PEG-G3-(Gd-DTPA)$_{11}$-(folate)$_5$ dendrimer.

overnight at room temperature. Methanol (10 mL) was added to quench the excess of anhydride and the reaction mixture was stirred for another 6 h. The reaction mixture was poured into excess of diethyl ether (700 mL) under vigorous stirring. A white powder separated was filtered and dried (yield, 95 %). Infrared spectroscopy (RX-1, Perkin Elmer, USA) and ^{1}H NMR (MQ-20, Bruker, Germany) were used to reveal the characterization of synthetic product.

Preparation of G_1 Generation of the PEG-dendrimer [PEG-bis[G-1]-$(OH)_2$] The PEG-bis[G-1]-(O_2Bn) (11.8 g) with protecting groups was dissolved in a mixture of methylene chloride and methanol (1:2). A mass of 1.18 g of Pd/C was added to the flask and the mixture was stirred in the presence of H_2 gas overnight. The Pd/C was filtered off through a short celite pad and the filtrate was poured into diethyl ether (600 mL). The hygroscopic white powder was filtered off quickly and dried under vacuum (yield, 90 %).

Preparation of Benzylidene-protected G_2 Generation of the PEG-dendrimer [PEG-bis[G-2]-$(O_2Bn)_2$] The second generation was prepared as described above. PEG-bis[G-1]-$(OH)_2$ (9.56 g, 0.83 mmol, 1 equiv) and DMAP (0.326 g, 2.6 mmol, 3.2 equiv) were dissolved in 25 mL of dichloromethane (DCM) and a solution of BOP-anhydride (5.69 g, 13.3 mmol, 16 equiv) in DCM (50 mL) was added drop wise and stirred overnight. The excess anhydride was quenched by the addition of methanol (15 mL) and the mixture was precipitated in diethyl ether. The white precipitate separated was filtered and dried under vacuum (yield, 80%).

Preparation of G_2 Generation of the PEG-dendrimer [PEG-bis[G-2]-$(OH)_4$] Deprotection of the compound PEG-bis[G-2]-(O_2Bn)$_2$ (5.5 g) was carried out by dissolving it in a 1:2 mixture of DCM and MeOH (60 mL) and by stirring with Pd/C in the presence of hydrogen gas for 24 h at room temperature. The reaction mixture was filtered through celite pad. A white hygroscopic powder was obtained upon precipitating the filtrate in diethyl ether (1 L; yield, 88%).

Preparation of Telechelic PEG-bis[G-3]-$(O_2Bn)_4$ The benzylidene-protected third generation of the dendrimer was prepared by stirring a mixture of PEG-bis[G-2]-$(OH)_4$ (2.88 g, 0.40 mmol, 1 equiv.), DMAP (0.3151 g, 2.57 mmol, 6.4 equiv.), and BOP-anhydride (5.48 g, 12.8 mmol, 32 equiv) in dichloromethane (100 mL) for 24 h at room temperature. The product was isolated as detailed in the case of G_2 and dried (yield, 89 %).

Preparation of G_3 Generation of the PEG-dendrimer [PEG-bis[G-3]-$(OH)_8$] The benzylidene-protected third generation of the dendrimer PEG-bis[G-3]-(O2Bn)$_4$ (4 g) was dissolved in 1:2 mixture of DCM:MeOH (60 mL) and was added Pd/C (0.40 g). The suspension was stirred under H_2 atmosphere for 24 h. The work-up as described for the other generations afforded the dendrimer as a white powder (yield, 76 %).

Preparation of the PEG-G3-$(Folate)_m$ A mixture of folic acid (13.76 mg, 5.76 mmol) and dicyclohexylcarbodiimide (DCC; 1.07 mg, 5.19 mmol) in dimethyl sulfoxide (DMSO; 20 mL) was stirred overnight at 50°C. Then, [PEG-bis[G-3]-$(OH)_8$] dendrimers (2.04 g, 0.36 mmol) was added. The resulting mixture was stirred for 24 h at 60°C to afford the dendrimer–folate conjugates. Free folic acid was removed by ultrafiltration using membrane of M.W. Co 1000. The yield of the reaction was 35% (0.97 g, 0.126 mmol). The folate content was then characterized by UV–Vis absorption spectroscopy (Libra S22, Biochrom, USA).

Preparation of the PEG-G3-$(Folate)_m$-$(DTPA)_n$ The folate-conjugated G_3 dendrimer (0.73 g, 0.0945 mmol) was then attached with DTPA units at the surface with DTPA-monoanhydride (1.56 g, 4.15 mmol) for 24 h in the presence of triethylamine (0.515 mL) at room temperature using DMSO (20 mL) as solvent. Free DTPA units were removed by ultrafiltration using membrane of M.W.CO 1000. The yield of the reaction was 80% (0.895 g, 0.075 mmol).

The content of DTPA groups was determined by a chelatometric titration method. A known weight of the dendrimer was dissolved in deionized water and ammonium buffer (pH 10) was added followed by a drop Eriochrome Black-T indicator. This mixture was titrated against 0.1 M calcium chloride solution until the blue color turns to reddish orange color.

Preparation of the PEG-G3-$(Folate)_m$-$(Gd\text{-}DTPA)_n$ The syntheses of gadolinium complexes of DTPA-terminated dendrimers were performed by adding the required equivalent of gadolinium salt ($GdCl_3 \cdot 6H_2O$) (0.29 g, 0.783 mmol) to the dendrimer (0.785 g, 0.0661 mmol) dissolved in demineralized water and by adjusting the pH between 6.0 and 6.5 using 1 N NaOH solution. Free gadolinium ions were removed by ultrafiltration using membrane of M.W.CO 1000. The yield of the reaction was 95% (0.86 g, 0.063 mmol).

The absence of free gadolinium ions were tested by using xylenol orange indicator at pH 5.8 (acetate buffer). The absence of uncomplexed DTPA unit was confirmed by adopting the titration method used to determine the number of DTPA units present in the dendrimer. The number of gadolinium ions doped was determined experimentally by using Inductively Coupled Plasma-Atomic Emission Spectroscopy (ICP-AES, S-35, Kontron, Germany). The complexes were filtered using a 0.45-μm filter and lyophilized.

T1 Relaxation Measurements The gadolinium-loaded dendrimers (0.2–1 mmol) were evaluated for their capacity to alter the relaxation rate of water using a NMR spectrometer (20 MHz, 0.47 T; MQ-20, Brucker, Germany) at 37°C with standard pulse program of inversion-recovery (range of TR, 0–300 ms).

The molecular weight of the PEG-G3-$(Gd\text{-}DTPA)_{11}$-$(folate)_5$ dendrimer is 12,556 Da. In addition, some dendrimers were labeled with fluorescein isothiocyanate (FITC) before the conjugation of Gd-DTPA and folate for cellular uptake experiments.

Cell Experiments

KB cells (ATCC, Manassas, VA) were used for folate-receptor-positive cells and HT-1080 cells (ATCC, Manassas, VA) were used for folate-receptor-negative cells, according to the literature [6]. Real-time PCR (RT-PCR) and immunohistochemistry were performed to reveal the FR expression level and the cellular uptake of FITC-labeled dendrimer was tested in KB and HT-1080 cells.

RT-PCR Total RNA was extracted from the KB and HT-1080 cells by Qiagen RNeasy kits (Qiagen, Hilden, Germany) and 1 μg of extracted total RNA was subjected to a reverse-transcription reaction using High-Capacity cDNA reverse Transcription Kits (Applied

Biosystems, Foster City, CA, USA). The complementary DNA from 20 ng of the total RNA was used as a template. GAPDH and folate receptor mRNA were quantified by a Sequence Detection System instrument (RPISM 7000, Applied Biosystems) using the TaqMan Gene Expression Assay (Applied Biosystems). The DNA sequence of FR primer and probe are: TGGANCAGA GCTGGCG, reverse primer: ACCCAGCCCAGGGCAA, probe: CCCTGTGCAAAGAG.

Immunohistochemistry After fixation of the KB and HT-1080 cells using 100% ethanol, the immunohistochemistry was performed using a mouse anti-human FR monoclonal antibody (ab3361, 1:50 dilution, Abcam, Cambridge, UK), revealed with biotinylated goat anti-mouse secondary antibody (NEF823, 1:250 dilution, PerkinElmer, MA,USA). The staining procedure was performed with a modified avidin–biotin–peroxidase complex technique (PK-6100, Vector Laboratories, Burlingame, CA, USA). The slides were visualized with the chromogen diaminobenzidine and counterstained with hematoxylin (Vector Laboratories). Control sections were processed identically, but with incubation with non-specific isotype immunoglobulin (Vector Laboratories).

Cellular Uptake of FITC-Labeled Dendrimer The KB and HT-1080 cells (5×10^4) were cultured on a cover glass overnight. FITC-labeled dendrimer (2 mM) was added into the culture medium for 2 h, then the cells were washed and fixed by 100% ethanol. DAPI (D8417, Sigma-Aldrich, Saint Louis, MO, USA) was used for nuclear staining. Slices were analyzed using a fluorescence microscope (Axioplan, Zeiss, Germany). Blue and green channels were used for DAPI and FITC fluorescence detection. Axiovision software (Zeiss) was used for image acquisition.

Free Folic Acid Competition and FR siRNA Knockdown In the cell uptake experiment, an additional set of 200-fold free folic acid (400 mM), was added to the culture medium as a competitor of the folate receptor before adding the FITC-labeled dendrimer (2 mM). In another setting, KB cells were first treated with FR-specific siRNA 48 h prior to cellular uptake study in order to suppress the FR expression of KB cells. FR-specific siRNA was commercially available and purchased from Ambion (NM_016724). Untreated KB cells were used for the positive control. RT-PCR was used to validate the success of the FR knockdown. Scrambled FR siRNA (Ambion) treated KB cells, were used as the negative control group, then the FR siRNA-treated KB cells, the scrambled FR siRNA-treated KB cells, and the normal KB cells, were used for the FITC-labeled dendrimer cellular uptake study.

Animal Preparation and Tumor Model

All animal studies were approved by the Institutional Animal Care Committee at our institution. Isoflurane inhalation was used for mice anesthesia. We delivered 1% for maintenance and 5% for induction in oxygen from a precision vaporizer (VIP3000, Midmark, Versailles, Ohio, USA). Carbon dioxide inhalation was used for euthanasia. NOD-SCID male mice (National Taiwan University Animal Center, Taipei, Taiwan), weighing 18–24 g (average weight 21.2 g) 8 weeks old, were handled in accordance with government guidelines.

To induce solid tumors, $1x10^6$ KB and HT-1080 cells were injected subcutaneously into the bilateral flank fat pads on the same mouse (KB: right flank, HT-1080: left flank) in 30 mice. Within 20-30 days after implantations, each mouse developed bilateral flank tumors of 12±5 mm in size. Mice were fed with a folate-free diet (TestDiet, Richmond, IN, USA) after there were visible tumors on bilateral flanks.

MR imaging

MR imaging of the mice was performed using a 1.5-T superconducting System (Powertrak 6000; Philips, Best, the Netherlands). A C4 surface coil was used. After the scout MR images were acquired, gradient echo T2-weighted coronal MR images ($TR/TE = 50/20$, flip angle=30, slice thickness/gap=2/0.2 mm, FOV 12 cm, NEX=2) were performed to reveal the extent of the bilateral flank tumors (KB tumor on the right flank and HT-1080 tumor on the left side). An axial dynamic contrast-enhanced MR image was then obtained with a section thickness of 2 mm, and a 12-cm FOV through the centers of the bilateral flank tumors. T1-weighted gradient-echo sequences (fast field echo; Philips) with $TR/TE = 188/3.4$, NEX=1, flip angle of 80°, and 179×256 acquisition matrix, were used. In total, 50 dynamic images were obtained within 30 minutes from each of the mice. A bolus (200ul) of $(Gd\text{-}DTPA)_{11}$-$(folate)_5$-PEG-cored dendrimer (0.1 mmol per kilogram of body weight) was administered manually through 31-gage needle, which was placed in the retrobulbar venous plexus of the mice before MR study and connected to a 300ul syringe through a polyethylene tube (PE-10, Becton. Dickinson and Co., USA). The dynamic contrast-enhanced MR imaging started before contrast injection, and was then observed for 30 minutes at different time intervals: 10 seconds (0-3 minutes), 30 seconds (3-10 minutes), 1 minutes (10-30 minutes).

Thirty mice bearing KB and HT1080 tumors were divided into three groups. Group 1 (n=18) was injected with the $(Gd\text{-}DTPA)_{11}$-$(folate)_5$-PEG-cored dendrimer (2 mmol/mouse). Group 2 (n=6) received $(Gd\text{-}DTPA)_{11}$-PEG-cored dendrimer without folate conjugation (2 mmol/mouse). Group 3 (n=6), was injected with a mixture of $(Gd\text{-}DTPA)_{11}$-$(folate)_5$-PEG-cored dendrimer (2 mmol/mouse), and 200-fold free folic acid (400 mmol folate/mouse).

Data Analysis

Signal intensity values were measured in operator-defined regions of interest (ROIs). The ROIs were placed by one investigator (W.T.C.), with the aid of a cursor and graphic display device, and encircled the entire tumor on an axial image through the bilateral tumor centers. Signal intensity (SI) was then measured for the KB and HT-1080 tumors. The SI values derived from the ROIs were plotted against time as a time–intensity curve (TIC) by a software system (Gyroview; Philips). The baseline value for signal intensity (SI_{base}) on a time–intensity curve was defined as the mean signal intensity from the first two images (Fig. 2). Three different phases were observed in TIC after contrast injection. The early arterial phase represents the first pass of contrast material into the lesions. The parenchymal phase represents the time period for the infiltration of the contrast material into the interstitial space of the lesions. The delayed phase observes the duration of contrast material retention after the parenchymal phase. The maximum signal intensity (SI_{max}) was defined as the peak enhancement value in the parenchymal phase. SI_{30min} was defined as the signal intensity measured 30 minutes after contrast injection. The contrast enhancement rise time (T_{rise}) was defined as the time between SI_{base} and SI_{max}. The contrast washout time ($T_{washout}$) was defined as the time

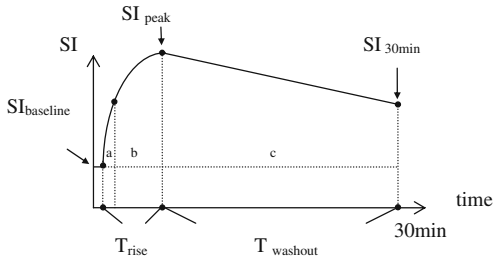

Fig. 2. Time–intensity curve of the dynamic contrast-enhanced MR study. Signal intensity of ROI was measured from 50 images for 30 min after contrast injection and plotted against time. Interval 'a': early arterial phase. Interval 'b': parenchymal phase. Interval 'c': delayed phase.

between SI_{max} and SI_{30min}. The peak enhancement percentages $[(SI_{max} - SI_{base})/SI_{base} \times 100\%]$, the 30-min contrast washout percentage $[(SI_{max} - SI_{30min})/SI_{base} \times 100\%]$, the enhancement slope, $[(SI_{max} - SI_{base})/(SI_{base} \times T_{rise}) \times 100\%]$, and the contrast washout slope $[(SI_{max} - SI_{30min})/(SI_{base} \times T_{washout}) \times 100\%]$ for each ROI were calculated and compared between the KB and HT-1080 tumors by *t* test. A receiver-operating characteristic curve (ROC) was used to determine the most appropriate cut-off point for the enhancement parameters. All statistics were analyzed using Stata 7.0 (Stata, College Station, TX, USA), for Windows (Microsoft, Redmond, WA, USA).

Patterns of TIC

The TICs were obtained by plotting the enhancement signal intensity over time (0–30 min). The TICs were classified into three types. Type A represents an initial rapidly rising slope followed by a second slow rising phase. Type B represents a rapidly rising slope (wash-in) during the early phase, followed by a plateau after the peak enhancement is achieved. Type C represents a rapidly rising slope (wash-in), the same as the upright portion of the type B curve, followed by a washout phase in the latter portion. If the difference of SI_{max} and the SI_{30min} is greater than 20% of baseline SI, the B curve will be defined as type A or C, depending on the wash-in or washout of the contrast material. The cut-off value was set at 20% because it is easier to observe in a TIC with such a scaling format [22]. Fisher's exact test was used to analyze the distribution of TIC patterns in the KB and HT-1080 tumors.

Results

Contrast Medium

Synthesis of [PEG-bis[G-3]-(OH)$_8$] The ^{1}H NMR spectrum of the BOP-protected G_3 dendrimer showed three singlets for three types of methyl protons at δ 0.93, 1.05, and δ 1.21 confirming the formation of three generations. The intensity ratio of the three types of methyl protons was 1:2:4, which confirmed the formation of three generations without structural truncation (Fig. 3). In the ^{1}H NMR spectrum of the PEG-bis[G-3]-$(OH)_8$, the spikes of G_1 and G_2 methyl protons merged together at δ 1.61 (Supplementary figure 2). However, the intensity ratio of the merged spike and the singlet of G_3 methyl protons was 3(1+2):4.

The formations of three generation were further confirmed by MALDI-TOF experiments. The observed values (calculated molecular weights are given parenthesis) for G_1, G_2, and G_3 are 4020 polydispersity (PDI): 1.01 (4232), 4900 PDI: 1.03 (4696), and 5572 PDI: 1.03 (5624), respectively.

Synthesis of the PEG-G$_3$-(Folate)$_5$ The number folate units attached were calculated from the UV–Vis spectroscopy, by comparing with the calibration curve obtained from known

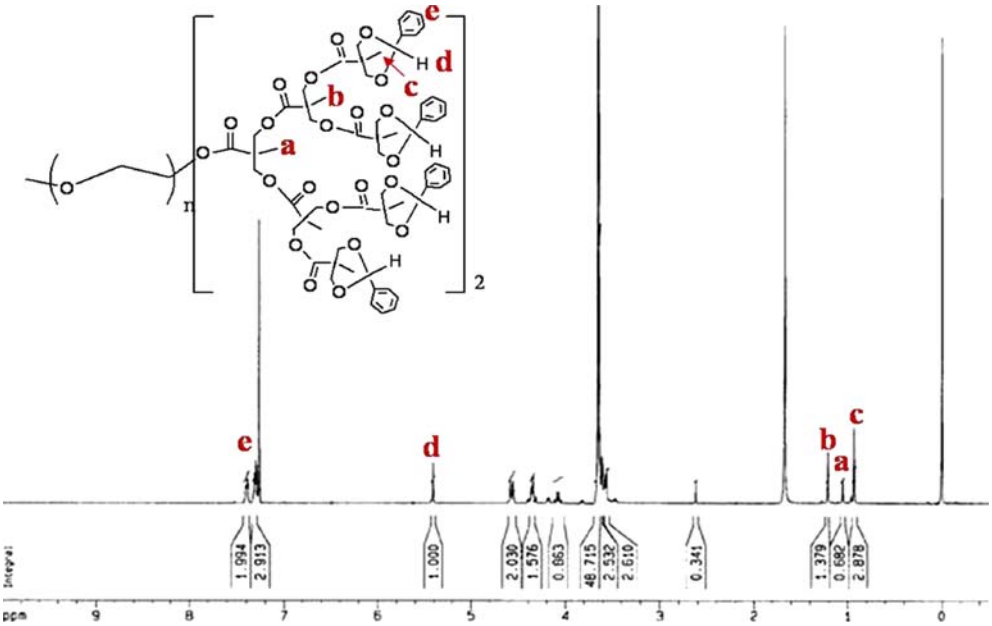

Fig. 3. The ^{1}H NMR spectrum of the BOP-protected G_3 dendrimer. Singlets *a*, *b*, *c* represented three types of methyl protons on G_1, G_2, and G_3 respectively. The intensity ratio of the three types of methyl protons was 1:2:4 (*a*:*b*:*c*), which confirmed the formation of three generations without structural truncation.

concentration of folate solutions. The average number of folate present in each mole of the G_3 generation dendrimer was calculated to be 5.1.

Synthesis of the PEG-G_3-(Folate)$_5$-(DTPA)$_{11}$ The number DTPA units attached were calculated from the volume of calcium chloride consumed. The average number of DTPA units present in each mole of the folate-attached G_3 dendrimer was calculated to be 11.

Synthesis of the PEG-G_3-(Folate)$_5$-(Gd-DTPA)$_{11}$ Structure elucidation of the gadolinium complexes by means of ^{1}H and ^{13}C NMR spectroscopy was complicated due to the paramagnetic nature of gadolinium. However, the formation of the dendrimer–gadolinium complexes could be confirmed with IR spectroscopy. IR spectroscopy demonstrated that the DTPA ligands were complexed with gadolinium, by the disappearance of the C–O stretching vibration around 1,200 cm^{-1} and the shift of the carbonyl stretch from 1,638 to 1,598 cm^{-1}. The number of gadolinium ions doped on each dendrimer was 10.5, calculated by ICP-AES. The chelatometric titration method also demonstrated that there was no unchelated DTPA unit on the dendrimer.

T1 Relaxation Measurements The gadolinium-loaded dendrimers were evaluated for their capacity to alter the relaxation rate of water using a NMR spectrometer (20 MHz, 0.47 T) with standard pulse program of inversion-recovery. The calculated r1 of the PEG-G3-(Gd-DTPA)$_{11}$-(folate)$_5$ was 4.8(mM S)$^{-1}$ per gadolinium [53.2 (mM S)$^{-1}$ per dendrimer].

Immunohistochemistry, RT-PCR and siRNA Experiments for Folate Receptor

The immunohistochemistry of folate receptor on KB and HT-1080 cells showed positive brown stain on KB cell surfaces (data not shown), negative stain on either HT-1080 cells, or on a non-specific immunoglobulin control slide. The folate receptor RT-PCR of KB and HT-1080 cells using GAPDH as internal control showed that the relative expression level of FR in KB cells was 2,048-fold higher than that in HT-1080 cells. The FR siRNA knockdown experiment showed the FR expression level was suppressed to 12.5% of the FR mRNA expression level of untreated KB cells, as revealed by RT-PCR. A cell viability test showed the FR siRNA-treated KB cells had the same viability as non-treated KB cells.

Cellular Uptake Experiments

After 2 h of incubation of the FITC-labeled dendrimer (2 mM) with KB cells, there were strong green fluorescence detected in KB cells by fluorescence microscopy (Axioplan, Zeiss, Germany; Fig. 4a,b). A free folate competition test was performed by adding 200-fold free folic acid (400 mM) into the culture medium before adding the FITC-labeled dendrimer; no green fluorescence was then detected in the FR-saturated KB cells (Fig. 4c,d). The FR siRNA-treated KB cells were incubated with the FITC-labeled dendrimer (2 mM) for 2 h, there was little green fluorescence detected by fluorescence microscopy(Fig. 6a–c), but green fluorescence was seen in the control GAPDH siRNA-treated KB cells (Fig. 4d–f). The HT-1080 cells showed negative green fluorescence in each situation (data not shown).

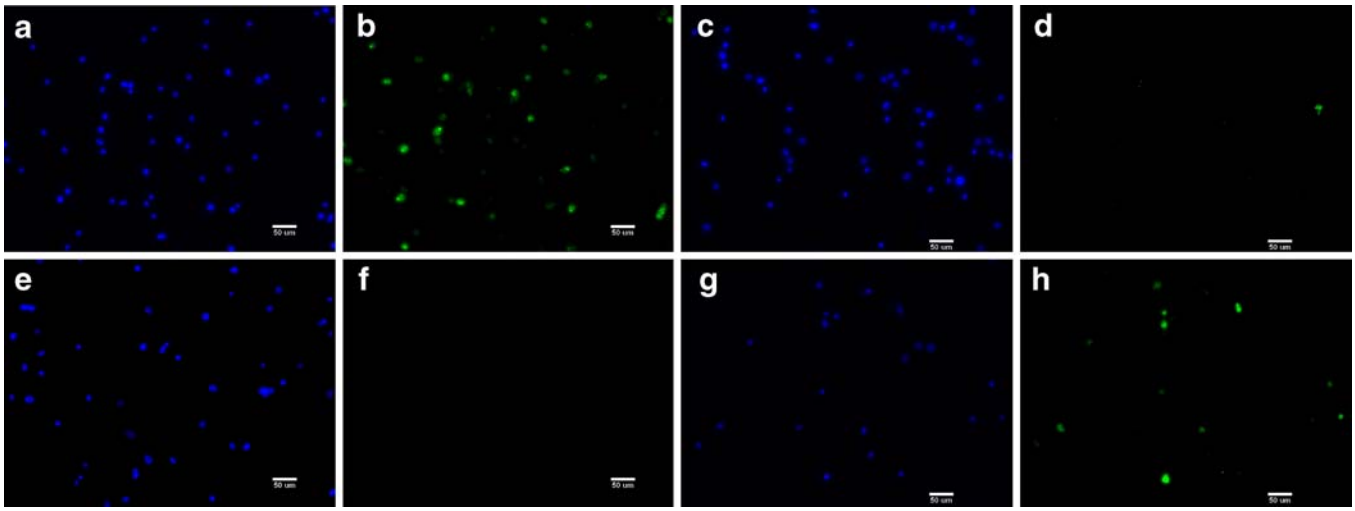

Fig. 4. **a–h** Cellular uptake experiments. Fluorescence microscopy was performed after incubation with the FITC-labeled folate-conjugated dendrimer for 2 h. **a**, **c**, **e**, **g**. Blue channel for DAPI nucleus staining in KB cells. **b**. Green channel for KB cells showed positive uptake of the dendrimer. **d**. Green channel for folic acid pre-saturated KB cells showed markedly decrease uptake of the dendrimer. **f**. Green channel for FR siRNA-treated KB cells showed decrease cellular uptake of the dendrimer. **h**. Green channel for GAPDH siRNA-treated KB cells showed positive cellular uptake of the dendrimer.

Contrast-Enhanced MR Imaging and Data Analysis

In NOD-SCID mice bearing KB, and HT-1080 tumors on bilateral flanks, the KB tumor showed a delayed contrast washout pattern (type A and B), after PEG-G3-(Gd-DTPA)$_{11}$-(folate)$_5$ i.v. injection, as compared to HT-1080 tumors (Fig. 5a,b). The average 30-min contrast washout percentage was −40±18% in KB tumors, 39±23% in HT-1080 tumors (n=18, p<0.001). After applying an ROC curve for the contrast washout percentage between KB and HT-1080 tumors, a 17% cut-off point was obtained to get a sensitivity of 94.4%, a specificity of 93.8%, and an accuracy of 94.1% for the diagnosis of FR-positive tumors (Fig. 6). The 30-min contrast washout slope also showed significant difference between the KB and HT-1080 tumors (−0.14± 0.78%/min versus 1.72±0.93%/min, p<0.001) in the PEG-G3-(Gd-DTPA)$_{11}$-(folate)$_5$ injection group. There was no

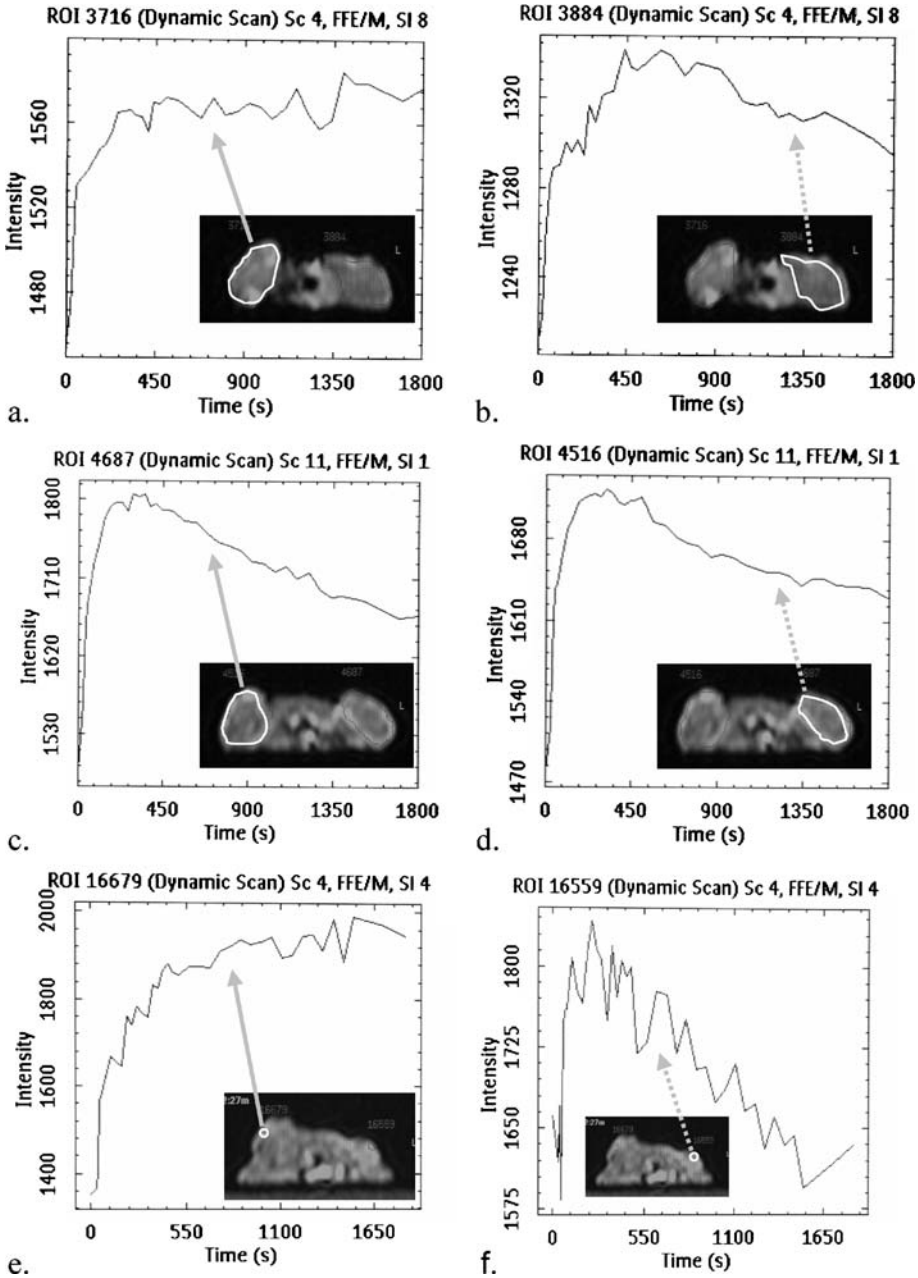

Fig. 5. **a**–**f** Time–intensity curve analysis. **a** The time–intensity curve for the dynamic-enhanced MRI (right: KB tumor; left :HT-1080 tumor) using PEG-G3-(Gd-DTPA)$_{11}$-(folate)$_5$. The KB tumor showed delayed contrast washout characteristics. **b** The HT-1080 tumor showed rapid contrast washout from the tumor after reaching peak enhancement. **c**, **d** The KB (*right*) and HT-1080 (*left*) tumors both showed early contrast washout characteristics after PEG-G3-(Gd-DTPA)$_{11}$ injection. **e** The peripheral zone of the KB tumor showed a gradual contrast fill-in phenomenon. **f** The peripheral zone of the HT-1080 tumor showed an early contrast washout pattern.

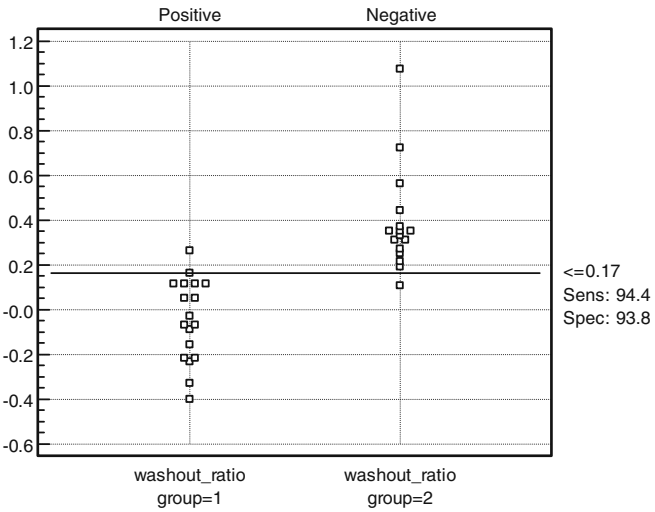

Fig. 6. The distribution of the 30-min contrast washout percentage in the KB and HT-1080 tumors. A 17% cut-off point was obtained to get a sensitivity of 94.4%, and a specificity of 93.8% for the diagnosis of FR-positive tumors.

significant enhancement percentage or enhancement slope difference between the KB and HT-1080 tumors in the PEG-G3-(Gd-DTPA)$_{11}$-(folate)$_5$ injection group. In the PEG-G3-(Gd-DTPA)$_{11}$ injection group (without folate conjugation), the enhancement percentage (58±9% versus 56±7%), the enhancement slope(15±3%/min versus 16±6%/min), the 30-min washout percentage (36±19% versus 38±27%) and the 30-min contrast washout slope (1.83±0.97%/min versus 1.79±0.88%/min) all showed no significant difference between the KB and HT-1080 tumors (n=6, p>0.05; Fig. 5c,d). If we focused on some peripheral-enhanced regions, we found an even more contrast fill-in characteristic in KB cells, but not in HT-1080 tumors (Fig. 5e,f). In a 200-fold free folic acid competition study, the enhancement pattern of KB tumors was the same as HT-1080 tumors (data not shown).

Patterns of TIC

The distribution of the three TIC patterns in the KB and HT-1080 tumors is listed in Table 1. All five type A curves were found in the KB tumors (Fig. 5a). Twelve (92.3%) of 13 type B curves were revealed in the KB tumors. Seventeen (94.4%) of 18 type C curves were seen in the HT-1080 tumors. There existed statistically significant different distribution of the TIC patterns between the KB and HT-1080 tumors (p<0.001), by Fisher's exact test.

Discussion

The folate receptor is a glycosylphosphatidylinositol-anchored membrane protein. It is overexpressed in most ovarian cancers, and a wide variety of other human cancers [1–4, 23]. In addition, FR is rarely expressed in normal tissues and FR has a high affinity with folate conjugates [8]. Therefore, folate-receptor-targeted drug delivery has been studied in recent years, which seems to enhance the treatment effect for FR-positive tumors [8, 24, 25]. Thus, there is an urgent need to develop a non-invasive imaging agent to determine if the tumor to be treated has folate receptors or not. Our study showed that it is feasible to identify FR-positive tumors by the 30-min contrast washout ratio of the PEG-G3-(Gd-DTPA)$_{11}$-(folate)$_5$ dendrimer, which is a new approach to MR molecular imaging.

Our results showed that a folate-conjugated macromolecule can be internalized by FR-positive cells and that such uptake can be suppressed by adding excessive free folic acid, or decreased in the FR siRNA-treated KB cells. In contrast-enhanced dynamic MR imaging, the FR-positive tumor was shown to have a delayed contrast washout phenomenon as compared to the FR-negative tumor. The specificity of this FR-targeting contrast agent was confirmed in a free folic acid competition study. Our data indicated that PEG-G3-(Gd-DTPA)$_{11}$-(folate)$_5$ has significant advantages for identifying FR-positive tumors. If we use 17% as a cut-off point, the sensitivity of diagnosis for FR-positive tumors was 94.4% and the specificity was 93.8%.

In this study, we classified the TICs into three types (A, B, C) by using a cut-off value of 20% subjectively. Seventeen (94.4%) of the 18 KB tumors were classified as having type A or B curves and 94.4% (17/18) of the HT-1080 tumors were classified as having type C curve by using such criteria. If the cut-off value was set to be smaller as 10%, all (18/18) of the HT-1080 tumors would then be classified as having type C curve, but 33.3% (six of 18) of the KB tumors would also fall into the type C curve category. The distribution of the type C curve will therefore be overlapped between the KB and HT-1808 tumors if we used a smaller cut-off value, although the contrast washout ratio was not distributed equally in these two kinds of tumors (KB tumors, 11%~26%; HT-1080 tumors, 11%~107%).

In order to obtain an unbiased comparison of perfusion parameters between contralateral tumors, we measured the entire cross-sectional area of each tumor. However, in our observation, the vascularity of the peripheral zone of the xenograft tumor was higher than the central zone. There was a peripheral enhancement pattern in both KB and HT-1080 tumors (Fig. 6a,b). If we applied a smaller ROI on the peripheral-enhanced regions of the KB tumors, some of them even showed a gradual contrast fill-in pattern during the 30 min after contrast injection (Fig. 6e,f). This

Table 1. Distribution of the enhancement patterns of the KB and HT-1080 tumors after PEG-G3-(Gd-DTPA)$_{11}$-(folate)$_5$ injection

	Type			Total
	A	B	C	
KB tumors	5	12	1	18
HT-1080 tumors		1	17	18
	5	13	18	36

phenomenon might be explained by focal increased vascular permeability so that the contrast medium might leak into the interstitial space, and gradually be internalized by the KB cells. Although a peripheral enhancement pattern also was observed with the HT-1080 tumors, their time–intensity curve also showed a rapid contrast washout phenomenon (Fig. 6b).

Contrast enhancement in MRI is induced by altering the relaxation status of the abundant water signal in tissue. This is done by employing either chelated Gd^{3+} to create T_1-positive contrast or superparamagnetic iron oxide particles to create T_2-negative contrast. The non-specific uptake of superparamagnetic iron particles by macrophages and reticuloendothelial system [26] could be a potential problem for the receptor-targeting purpose. Thus, we prefer using T_1-positive contrast agents in the receptor-targeted MR imaging experiments.

The detection of MR contrast accumulation in lesions is less sensitive than nuclear medicine [27]. Due to the small molecular size, the clinically used Gd-DTPA excretes rapidly through the kidney, which produces a rapid decrease in tissue Gd concentration and limits its clinical usage for receptor-targeted imaging [28]. The folate-conjugated macromolecule, carrying a varied number of gadolinium ions, had several advantages. First, due to its larger molecular size, it can stay longer in the blood stream, and has more opportunity to be incorporated by the receptor-positive tumors. Second, it contains more receptor probes per molecule for the targeting purpose. Third, it can increase its T1 relaxation by carrying several gadolinium chelates on one macromolecule [29]. Our dendrimer has 16 hydroxyl functional groups, which carried an average of eleven Gd-DTPA units for MR signal magnification. The r1 of our contrast agent was $4.8(\text{mM S})^{-1}$ per gadolinium, which is 1.67-fold higher than Gd-DTPA [$2.9(\text{mM S})^{-1}$]. Our results demonstrated the beneficial effect of increased T1 relaxicity per gadolinium by using dendrimeric Gd chelates [29]. Our study is a proof-of principle study, and our results showed that this strategy is applicable for receptor-targeting MR imaging.

In the pilot study, we tried to apply conventional post-contrast T1 MR images and compared the enhancement ratio of the FR-positive and -negative tumors at various time points (4, 8, 12, and 24 h...) after contrast injection, as other authors did in previous receptor-targeted MR studies [15, 30]. However, we found that it was difficult to get exactly the same imaging plane of the tumors once we re-arranged the mouse position and the baseline MR signal intensity fluctuated at various time points due to MR unit internal variability. In a clinical situation, it also might not be practical to follow the same patient for such a long period. Furthermore, there will be no negative control tumor for comparison in clinical situations. Our study demonstrated that dynamic contrast-enhanced MRI can avoid positional change bias, qualitatively measure pharmacokinetic characteristics of the agent, and the 30-min contrast washout percentage can be used as an independent parameter to predict FR-positive tumors. To our knowledge, this kind of approach has not been proposed in previous receptor-targeted MR imaging studies.

Although the tail vein injection is a traditional way to perform i.v. injections for mice, it is sometimes difficult to maintain a stable i.v. route before and during contrast injection via the tail vein. A retrobulbar venous plexus injection was proposed by Bathke [31], due to the retrobulbar venous plexus being relatively large with a thick wall, and the micro-needle can be fixed by periorbital fat pads. We found it is an applicable and stable i.v. route which can be easily settled before the MR study, and the mouse can be safely transferred to an MR gantry and receive dynamic contrast-enhanced MR examinations without any positional change before and after contrast injection. This gives a non-bias observation of the hemodynamic characteristics of a specific portion of the tumor.

The main disadvantage of this study was that we used a 1.5-T MR magnet for mice tumor imaging. The imaging resolution (0.47 mm/pixel), signal-to-noise ratio, and contrast-to-noise ratio, was not as good as high magnetic MR units designed for small animals. However, the average tumor size was 1.2 cm in our study (range from 0.7–1.6 cm). This range of tumor size can be clearly revealed by a 1.5-T MR magnet by using a small wrist surface coil. Another drawback of this study is that we did not measure the enhancement ratio longer than 30 min, but our approach might be more practical in future clinical situations after stringent investigation of cytoxicity of this agent, and avoid positional change bias at various time points.

This study showed that a PEG-cored dendrimer carrying gadolinium chelates and folates can be used in MR imaging to diagnose FR-positive tumors in a mouse xenograft model. The 30-minute contrast washout percentage obtained from the dynamic contrast-enhanced MRI is a useful parameter for the diagnosis of FR-positive tumors. This approach may therefore represent a step toward the diagnosis of folate-positive tumors and future individual medicine.

Acknowledgments. This research was supported in part by National Science Council grants 95-2314-B-532-005 and 96-2321-B-532-0001. We thank Mr. Hsiau Yu Yo and Mr. Wei Ju Hsu for their diligent laboratory work.

References

1. Campbell IG, Jones TA, Foulkes WD, Trowsdale J (1991) Folate-binding protein is a marker for ovarian cancer. Cancer Res 51:5329–5338
2. Wu M, Gunning W, Ratnam M (1999) Expression of folate receptor type alpha in relation to cell type, malignancy, and differentiation in ovary, uterus, and cervix. Cancer Epidemiol Biomarkers Prev 8:775–782
3. Iwakiri S, Sonobe M, Nagai S et al (2008) Expression status of folate receptor alpha is significantly correlated with prognosis in non-small-cell lung cancers. Ann Surg Oncol 15:889–899
4. Parker N, Turk MJ, Westrick E et al (2005) Folate receptor expression in carcinomas and normal tissues determined by a quantitative radioligand binding assay. Anal Biochem 338:284–293
5. Antony AC (1992) The biological chemistry of folate receptors. Blood 79:2807–2820

6. Lee RJ, Low PS (1994) Delivery of liposomes into cultured KB cells via folate receptor-mediated endocytosis. J Biol Chem 269:3198–3204
7. Mathias CJ, Wang S, Lee RJ et al (1996) Tumor-selective radiopharmaceutical targeting via receptor-mediated endocytosis of gallium-67-deferoxamine-folate. J Nucl Med 37:1003–1008
8. Leamon CP, Low PS (2001) Folate-mediated targeting: from diagnostics to drug and gene delivery. Drug Discov Today 6:44–51
9. McHugh M, Cheng YC (1979) Demonstration of a high affinity folate binder in human cell membranes and its characterization in cultured human KB cells. J Biol Chem 254:11312–11318
10. Hu XF, Xing PX (2003) Discovery and validation of new molecular targets for ovarian cancer. Curr Opin Mol Ther 5:625–630
11. Bettio A, Honer M, Muller C et al (2006) Synthesis and preclinical evaluation of a folic acid derivative labeled with 18F for PET imaging of folate receptor-positive tumors. J Nucl Med 47:1153–1160
12. Saborowski O, Simon GH, Raatschen HJ et al (2007) MR imaging of antigen-induced arthritis with a new, folate receptor-targeted contrast agent. Contrast Media Mol Imaging 2:72–81
13. Sun C, Sze R, Zhang M (2006) Folic acid-PEG conjugated superparamagnetic nanoparticles for targeted cellular uptake and detection by MRI. J Biomed Mater Res A 78:550–557
14. Swanson SD, Kukowska-Latallo JF, Patri AK et al (2008) Targeted gadolinium-loaded dendrimer nanoparticles for tumor-specific magnetic resonance contrast enhancement. Int J Nanomedicine 3:201–210
15. Konda SD, Aref M, Wang S, Brechbiel M, Wiener EC (2001) Specific targeting of folate-dendrimer MRI contrast agents to the high affinity folate receptor expressed in ovarian tumor xenografts. MAGMA 12:104–113
16. Artemov D, Mori N, Ravi R, Bhujwalla ZM (2003) Magnetic resonance molecular imaging of the HER-2/neu receptor. Cancer Res 63:2723–2727
17. Towner RA, Smith N, Doblas S et al (2008) *In vivo* detection of c-Met expression in a rat C6 glioma model. J Cell Mol Med 12:174–186
18. Chen TJ, Cheng TH, Hung YC et al (2008) Targeted folic acid-PEG nanoparticles for noninvasive imaging of folate receptor by MRI. J Biomed Mater Res A 87:165–175
19. Kawashima H, Matsui O, Suzuki M et al (2000) Breast cancer in dense breast: detection with contrast-enhanced dynamic MR imaging. J Magn Reson Imaging 11:233–243
20. Muramoto S, Uematsu H, Kimura H et al (2002) Differentiation of prostate cancer from benign prostate hypertrophy using dual-echo dynamic contrast MR imaging. Eur J Radiol 44:52–58
21. Ihre H, Padilla De Jesus OL, Frechet JM (2001) Fast and convenient divergent synthesis of aliphatic ester dendrimers by anhydride coupling. J Am Chem Soc 123:5908–5917
22. Chen WT, Shih TT, Chen RC et al (2002) Blood perfusion of vertebral lesions evaluated with gadolinium-enhanced dynamic MRI: in comparison with compression fracture and metastasis. J Magn Reson Imaging 15:308–314
23. Holm J, Hansen SI, Hoier-Madsen M, Birn H, Helkjaer PE (1999) High-affinity folate receptor in human ovary, serous ovarian adenocarcinoma, and ascites: radioligand binding mechanism, molecular size, ionic properties, hydrophobic domain, and immunoreactivity. Arch Biochem Biophys 366:183–191
24. Leamon CP, Reddy JA (2004) Folate-targeted chemotherapy. Adv Drug Deliv Rev 56:1127–1141
25. Wang S, Low PS (1998) Folate-mediated targeting of antineoplastic drugs, imaging agents, and nucleic acids to cancer cells. J Control Release 53:39–48
26. Beduneau A, Ma Z, Grotepas CB et al (2009) Facilitated monocyte-macrophage uptake and tissue distribution of superparmagnetic iron-oxide nanoparticles. PLoS ONE 4:e4343
27. Glunde K, Bhujwalla ZM (2008) Will magnetic resonance imaging (MRI)-based contrast agents for molecular receptor imaging make their way into the clinic? J Cell Mol Med 12:187–188
28. Brasch RC (1991) Rationale and applications for macromolecular Gd-based contrast agents. Magn Reson Med 22:282–287 discussion 300-283
29. Zhou XL, Zhi; Tang, Dazong; Xia, Liming; Meng, Liping; Xiang, Guangya. (2007) Preparation of targeted Gd3+ contrast agent based on folate—receptor and its relaxation. Zhongguo Yaoxue Zazhi 42:1640–1644
30. Yuan Z, Liu SY, Xiao XS, Zhong GR, Jiang QJ (2007) Folate-poly-L-lysine-Gd-DTPA as MR contrast agent for tumor imaging via folate receptor-targeted delivery. Zhonghua Yi Xue Za Zhi 87:673–678
31. Bathke W (1967) On intravenous injections into the retrobulbar venous plexus of white mice in bacteriological studies. Z Med Labortech 8:318–321
32. Weissleder R, Mahmood U (2001) Molecular imaging. Radiology 219:316–333